ADVANCED FUNCTIONAL MATERIALS
www.afm-journal.de

Materials Views
www.MaterialsViews.com

High-Performance Air-Stable n-Type Organic Transistors Based on Core-Chlorinated Naphthalene Tetracarboxylic Diimides

By *Joon Hak Oh, Sabin–Lucian Suraru, Wen-Ya Lee, Martin Könemann, Hans Wolfgang Höffken, Cornelia Röger, Rüdiger Schmidt, Yoonyoung Chung, Wen-Chang Chen, Frank Würthner,** and *Zhenan Bao**

Core-chlorinated naphthalene tetracarboxylic diimides (NDIs) with fluoroalkyl chains are synthesized and employed for n-channel organic thin-film transistors (OTFTs). Structural analyses of the single crystals and thin films are performed and their charge-transport behavior is investigated in terms of structure–property relationships. NDIs with two chlorine substituents are shown to exhibit a herringbone structure with a very close π-plane distance (3.3–3.4 Å), a large π-stack overlap (slipping angle ca. 62°), and high crystal densities (2.046–2.091 g cm^{-3}). These features result in excellent field-effect mobilities of up to 1.43 cm^2 V^{-1} s^{-1} with minimal hysteresis and high on–off ratios (ca. 10^7) in air. This is similar to the highest n-channel mobilities in air reported so far. Despite the repulsive interactions of bulky Cl substituents, tetrachlorinated NDIs adopt a slip-stacked face-to-face packing with an interplanar distance of around 3.4 Å, resulting in a high mobility (up to 0.44 cm^2 V^{-1} s^{-1}). The air-stability of dichlorinated NDIs is superior to that of tetrachlorinated NDIs, despite of their higher LUMO levels. This is closely related to the denser packing of the fluorocarbon chains of dichlorinated NDIs, which serves as a kinetic barrier to the diffusion of ambient oxidants. Interestingly, these NDIs show an optimal performance either on bare SiO_2 or on octadecyltrimethoxysilane (OTS)-treated SiO_2, depending on the carbon number of the fluoroalkyl chains. Their synthetic simplicity and processing versatility combined with their high performance make these semiconductors highly promising for practical applications in flexible electronics.

1. Introduction

Organic thin-film transistors (OTFTs) have attracted a great deal of attention as they are promising components for low-cost, large-area, and flexible electronics.[1–6] However, the difficulty in finding high-performance n-channel organic semiconductors that hold both a high charge-carrier mobility and ambient stability, has been a significant hurdle for their use in complementary circuits offering low-power dissipation, greater operating speed, and more stable operation. Despite the recent remarkable progress in the molecular design and device performance of n-channel semiconductors,[7–18] the development of high-mobility, air-stable n-channel organic semiconductors, in particular those with synthetic simplicity and versatile processing, remains a challenge.

Naphthalene tetracarboxylic diimides (NDIs), which can be easily synthesized from commercially available naphthalene tetracarboxylic dianhydrides (NDAs), are among the most promising n-channel candidates because of their high electron affinity and tunability of the optoelectronic property.[7,9,19,20] It is well known that the substituents at the imide nitrogens of the NDI greatly affect the molecular packing motif, thin-film morphology, and charge-carrier mobility.[21,22] Shukla et al. reported that cyclohexyl end groups in NDI increase the conformational rigidity of the overall molecule and assist in directing intermolecular stacking, leading to a high field-effect mobility near 6 cm^2 V^{-1} s^{-1}.[23] However, bis(cyclohexyl)-NDI based OTFTs are not stable in air because of the relatively high energy level

[*] Prof. Z. Bao, Dr. J. H. Oh,[+] Dr. W.-Y. Lee
Department of Chemical Engineering, Stanford University
Stanford, CA 94305 (USA)
E-mail: zbao@stanford.edu
Prof. F. Würthner, S.-L. Suraru, Dr. C. Röger, Dr. R. Schmidt
Institut für Organische Chemie, Universität Würzburg
Am Hubland, D-97074 Würzburg (Germany)
E-mail: wuerthner@chemie.uni-wuerzburg.de
Dr. M. Könemann, H. W. Höffken
BASF SE, GVP/C and GVC/C A030
D-67056 Ludwigshafen (Germany)
Y. Chung
Department of Electrical Engineering, Stanford University
Stanford, CA 94305 (USA)
Prof. W.-C Chen, Dr. W.-Y Lee
Department of Chemical Engineering, National Taiwan University
Taipei 106 (Taiwan)

[+] Current address: School of Nano-Biotechnology and Chemical Engineering, Ulsan National Institute of Science and Technology (UNIST), Ulsan 689-798 (Korea)

DOI: 10.1002/adfm.201000425

of the lowest unoccupied molecular orbital (LUMO). The ambient stability of OTFTs based on arylene diimide semiconductors can be improved by substitution with strong electron-withdrawing groups, such as F,[16,18,24] CN,[12] alkanoyl,[25] perfluorobenzene,[26] and fluoroalkyl groups,[9,27] either at the imide position or at the NDI core. This yields air-stable n-channel operation by significantly lowering the LUMO of the resulting molecule, which aids in resisting ambient oxidation. In addition, the self-segregation of densely packed fluorocarbon chains has been shown to provide a kinetic barrier to the diffusion of ambient oxidants such as oxygen, moisture, and ozone into the active channel area.[1,12,17–19] Recently it has been demonstrated that the interplay between the energetic and kinetic factors plays an important role in the air-stability of n-channel OTFTs.[28]

Chlorination has, so far, been less explored as a means to create air-stable n-channel OTFTs compared to the aforementioned substitutions with electron-withdrawing groups. However, our recent results[29,30] showed that despite the relatively low electronegativity of the Cl atoms, chlorinated molecules typically have a lower LUMO than their fluorinated counterparts for undistorted π-conjugated core systems because of delocalization of π-electrons into the unoccupied 3d orbitals, which are not available with F atoms. Therefore, chlorination is a viable route towards n-channel OTFTs. Chlorinated compounds are synthetically more accessible and have a relatively lower precursor cost.

For this work, we synthesized four core-chlorinated NDI compounds with fluorinated side chains at the imide positions and we characterized the electrical properties of the n-channel OTFTs. For comparison, a parent molecule without chlorine substitution was also synthesized and its TFT performance was examined. To elucidate the effects of successive core substitutions, we introduced two or four chlorine substituents in the core region. Two different fluoroalkyl chains were also introduced at the imide nitrogen to improve the ambient stability of the NDI TFTs. We studied their structure–property correlations by investigating the thin-film growth, molecular packing, orbital energies, and field-effect mobilities.

2. Results and Discussion

2.1. Synthesis

The NDI derivatives were synthesized according to Scheme 1. The detailed conditions for the synthetic procedures are included in the Supporting Information. Briefly, 1,4,5,8-naphthalene tetracarboxylic dianhydride (**1a**) was heated under reflux in quinoline together with zinc acetate and 2,2,3,3,4,4,4-heptafluorobutylamine or 2,2,3,3,4,4,5,5,5-nonafluoropentylamine, respectively, to yield compounds **2a** and **2b**. Whereas **2b** was only isolated in its crude form as a synthetic intermediate, compound **2a** was further purified by column chromatography to give a slightly yellowish powder (71% yield). 2,6-Dichloronaphthalene tetracarboxylic dianhydride (**1b**) was prepared according to the literature,[31] and heated under reflux in acetic acid with 2,2,3,3,4,4,4-heptafluorobutylamine by 2,2,3,3,4,4,5,5,5-nonafluoropentylamine to yield yellowish solids **3a** (47% yield) and **3b** (55% yield), respectively. For the synthesis of tetrachlorinated NDI **4a**, a mixture of **2a**, chlorosulfonic acid, and iodine was heated to 85 °C under Cl_2 flow. After recrystallization from dichloromethane, **4a** was obtained in 49% yield. Similarly, **4b** was obtained in 70% yield from **2b**. The NDI compounds were purified by vacuum sublimation in a three-temperature-zone furnace before thin-film deposition.

2.2. Electronic Structure Characterization

The energy levels of the core-chlorinated NDIs were investigated both in solution and in thin film. The cyclic voltammetry results show two reversible reduction waves for the NDIs, whereas no oxidation wave could be observed because of the limited available potential range in the given solvent (see Fig. S1 in the Supporting Information).[18] The successive chlorination in the core region gradually lowered the LUMO levels of the NDI derivatives. For instance, compound **2a** without Cl substitution at the core showed

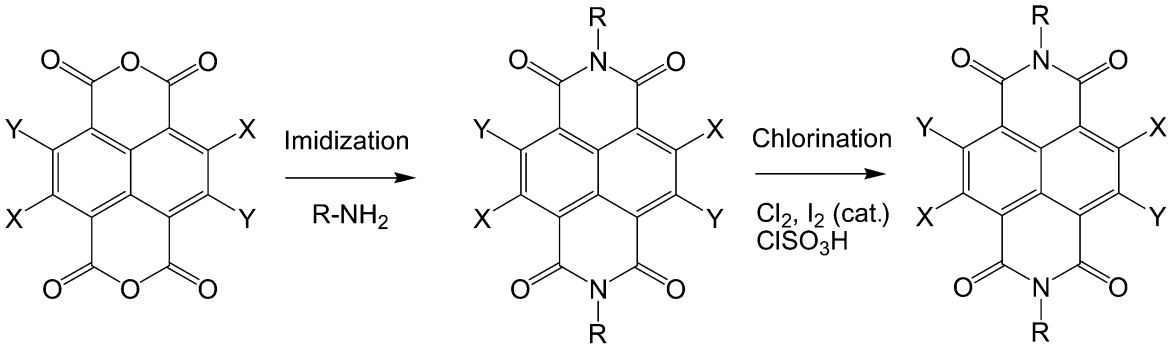

1a: X=Y=H
1b: X=H, Y=Cl

2a: X=Y=H; R=$CH_2C_3F_7$
2b: X=Y=H; R=$CH_2C_4F_9$

3a: X=H, Y=Cl; R=$CH_2C_3F_7$
3b: X=H, Y=Cl; R=$CH_2C_4F_9$

4a: X=Y=Cl; R=$CH_2C_3F_7$
4b: X=Y=Cl; R=$CH_2C_4F_9$

Scheme 1. Synthesis of core-chlorinated NDIs.

a LUMO of –3.72 eV, while **4a** with four Cl substituents exhibited a much lower LUMO of –4.13 eV. The shift in the LUMO level (0.41 eV) for the NDIs was much larger than that (0.13 eV) for perylene tetracarboxylic diimides (PDIs) after tetrachlorination of the core.[30,32] The distortion of the NDI core (dihedral angles $\leq 7^{\circ}$) is much less than that of the PDI core (ca. 35°) after core-tetrachlorination, which leads to the relatively easier delocalization of electrons in the NDI π-conjugated core.

Figure 1 shows the UV-vis spectra obtained from NDIs in solution and in thin films. The bandgap (E_g) was reduced with increasing degree of chlorination, as shown by the red shift of the long-wavelength absorption edge in the UV-vis spectra. This mainly originated from the lowering of the LUMO levels. However, the LUMO and bandgap were less sensitive than expected to the length of the fluorinated side chains. (Note that the UV-vis spectra of NDIs with the same degree of core-chlorination were similar.) We performed ultraviolet photoelectron spectroscopy (UPS) to investigate the ionization potential of the thin films. Unfortunately, we could not observe any signals with a reasonably high intensity from the NDI thin films. Density functional theory (DFT) calculations were performed at the B3LYP level of theory with a 6-31G* basis set using the Gaussian03[33] program. The calculated orbital energies and the tendency of decreasing LUMO energy with increasing chlorination are in good agreement with the experimentally obtained results (see Table 1).

2.3. OTFT Characterization

The deposition conditions of NDI molecules were optimized by examining various substrate temperatures (T_D) (25, 50, and 70 °C) and different surfaces, namely, bare SiO_2/Si or OTS-treated SiO_2/Si substrates. Table 2 summarizes the performance of the NDI-based OTFTs under optimized conditions (see Table S1 for the performance details under other conditions). Figure 2 shows transfer curves and plots of $(I_{DS})^{1/2}$ vs. V_{GS} for the NDI OTFTs fabricated under the best performing conditions. The highest mobility (0.38 $cm^2 V^{-1} s^{-1}$) of the parent core-unsubstituted NDI **2a** on an OTS-treated surface was around 40 times higher than that reported for the same films on untreated SiO_2/Si substrates (0.01 $cm^2 V^{-1} s^{-1}$) at the same T_D of 25 °C, with a three orders of magnitude higher on–off current ratio (I_{on}/I_{off}) (10^7).[9,19] This is presumably related to the highly ordered, crystalline nature of the OTS layer, which effectively eliminates surface traps.[34] At a higher T_D of 50 °C, thin films of **2a** on an OTS-treated SiO_2/Si substrate yielded a mobility of 0.01 $cm^2 V^{-1} s^{-1}$, whereas no field-effect

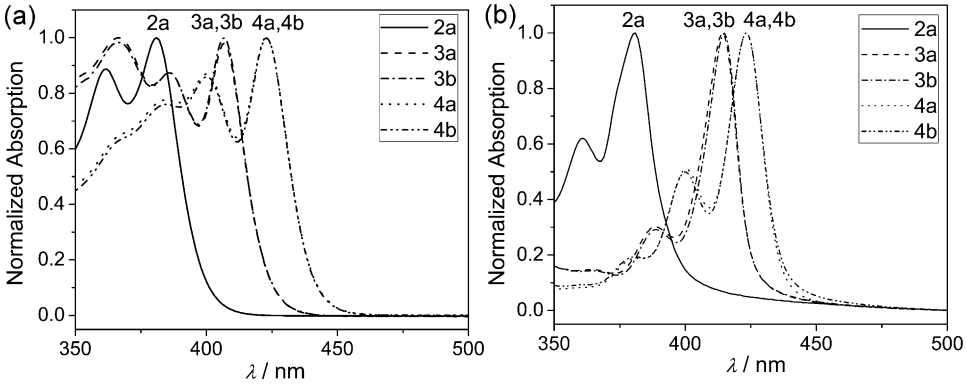

Figure 1. UV-vis spectra of core-chlorinated NDIs in a) *o*-dichlorobenzene and b) 45-nm-thick thin films prepared under device fabrication conditions. The UV-vis spectra of the parent core-unsubstituted NDI **2a** are presented for comparison.

Table 1. Summary of the λ_{max} of UV-vis spectra in solution and thin film, HOMO/LUMO in solution, bandgap in solution and in the thin film, and the HOMO/LUMO levels predicted by DFT calculations for the NDIs.

Semiconductor	Solution				Thin Film [e]		DFT calc. [g]	
	λ_{MAX}[a] [nm]	HOMO[b] [eV]	LUMO[c] [eV]	E_g[d] [eV]	λ_{MAX} [nm]	E_g[f] [eV]	HOMO [eV]	LUMO [eV]
2a	381	−6.84	−3.72	3.12	381	3.13	−7.36	−3.73
3a	407	−6.92	−4.01	2.91	414	2.91	−7.48	−3.93
3b	407	−6.92	−4.01	2.91	415	2.91	−7.48	−3.94
4a	423	−6.94	−4.13	2.81	423	2.84	−7.59	−4.05
4b	423	−6.95	−4.14	2.81	423	2.84	−7.59	−4.06

[a] λ_{max} measured in *o*-dichlorobenzene. [b] HOMO estimated from LUMO and E_g. [c] LUMO measured by cyclic voltammetry in degassed CH_2Cl_2 with 0.1 M $TBAFPF_6$ as the electrolyte, with respect to a Fc/Fc^+ reference (−4.8 eV to vacuum) added after each measurement. [d] E_g (eV), bandgap in solution obtained from the long wavelength absorption edge. [e] 45-nm thin film prepared by evaporation under high vacuum. [f] E_g of the thin film on quartz obtained from the long wavelength absorption edge. [g] DFT calculations using Gaussian03 with the B3LYP level of theory and 6-31G* basis set.

Table 2. Summary of the performance for the NDI-based TFTs prepared under optimized conditions.

NDI	T_D [°C]	Surf.	In N_2			In air			
			μ [$cm^2V^{-1}s^{-1}$] [a]	I_{on}/I_{off}	V_T [V]	μ [$cm^2V^{-1}s^{-1}$]	I_{on}/I_{off}	V_T [V]	$\Delta\mu$ [%][b]
2a	25	OTS	0.34 ± 0.03 (0.38)[c]	$(1.3 \pm 0.4) \times 10^7$	28 ± 4	0.26 ± 0.02 (0.27)	$(1.3 \pm 0.1) \times 10^7$	19 ± 1	−23.5
3a	50	Bare	0.70 ± 0.09 (0.86)	$(5.3 \pm 1.3) \times 10^5$	20 ± 1	0.75 ± 0.13 (0.91)	$(3.8 \pm 1.7) \times 10^6$	25 ± 2	+7.1
3b	70	OTS	1.12 ± 0.10 (1.26)	$(2.2 \pm 0.9) \times 10^7$	15 ± 2	1.32 ± 0.10 (1.43)	$(5.3 \pm 0.6) \times 10^7$	23 ± 2	+17.9
4a	50	Bare	0.15 ± 0.003 (0.15)	$(1.5 \pm 0.3) \times 10^6$	32 ± 1	0.019 ± 0.016 (0.021)	$(2.6 \pm 2.4) \times 10^5$	22 ± 5	−87.3
4b	70	OTS	0.34 ± 0.11 (0.44)	$(2.1 \pm 2.0) \times 10^6$	53 ± 1	0.036 ± 0.003 (0.040)	$(2.2 \pm 1.2) \times 10^7$	40 ± 1	−89.4

[a] Average values obtained for at least 3 devices. [b] Variation of mobilities in N_2 and in air (ca. 1 h exposure). [c] Maximum mobility recorded. **2a** was desorbed at a T_D higher than 50 °C under vacuum conditions (ca. 1×10^{-6} Torr). The core-chlorinated NDIs were desorbed at $T_D = 90$ °C.

behavior was observed for those on bare SiO_2/Si substrates because of desorption. At $T_D = 25$ °C, OTFT devices of dichlorinated **3a** on OTS-treated SiO_2/Si substrates also showed a higher mobility compared to those on bare SiO_2/Si substrates. However, the field-effect mobility of **3a** on a bare SiO_2/Si substrate increased by more than two orders of magnitude upon heating the substrate from 25 °C to 50 °C during deposition, leading to a higher mobility (up to 0.86 $cm^2 V^{-1} s^{-1}$) for the device fabricated at 50 °C. The tetrachlorinated NDI, **4a** exhibited a decreased mobility by an order of magnitude compared to that of **3a**, which has two Cl substituents at the core position. This may be related to a larger stacking distance between the NDI dyes (reduced π–π orbital overlap) of **4a** because of a more distorted NDI core. TFT devices of **4a** exhibited the highest mobility (0.15 $cm^2 V^{-1} s^{-1}$) on a bare SiO_2/Si substrate after deposition at 50 °C.

Among the synthesized NDIs, compound **3b** with two Cl substituents at the core and a $-CH_2C_4F_9$ group at the imide nitrogen yielded the best performing TFTs on the OTS-treated SiO_2/Si substrate at $T_D = 70$ °C, with the highest mobilities both in N_2 (1.26 $cm^2 V^{-1} s^{-1}$) and in air (1.43 $cm^2 V^{-1} s^{-1}$), with an I_{on}/I_{off}

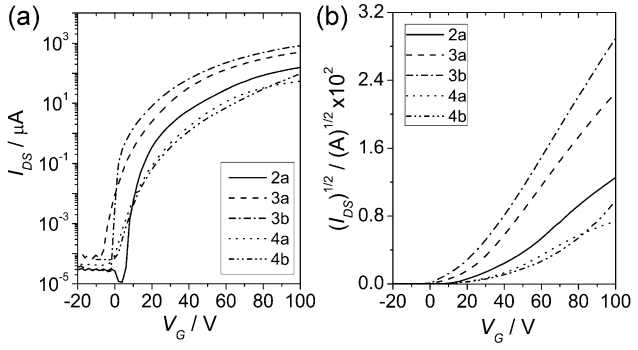

Figure 2. Representative *I–V* characteristics of NDI TFTs fabricated under the best performing conditions. a) Comparison of the transfer curves and b) comparison of the plots of $(I_{DS})^{1/2}$ vs. V_{GS}. Thin-film deposition conditions: **2a**: 25 °C, OTS-treated SiO_2/Si substrate; **3a**: 50 °C, bare SiO_2/Si substrate; **3b**: 70 °C, OTS-treated SiO_2/Si substrate; **4a**: 50 °C, bare SiO_2/Si substrate; **4b**: 70 °C, OTS-treated SiO_2/Si substrate.

ratio as high as 10^7, and a threshold voltage (V_T) of about 20 V. This mobility is among the highest reported for air-stable n-channel OTFTs. As can be seen from the relative variation of mobilities ($\Delta\mu$) in Table 2, the initial mobilities of several TFT devices prepared from dichlorinated NDIs **3a** and **3b** were rather higher in air, despite the slightly lower on-currents in air compared to those in N_2. This presumably originates from the V_T shift in positive direction by charge-carrier trapping and the increased I_{on}/I_{off} because of the oxidation of unintentionally doped NDI radical anions in air.[17] After exposing the TFT devices to air for 3 months, the average mobilities of the devices of **2a**, **3a**, **3b**, **4a**, and **4b** decreased from 0.34, 0.70, 1.12, 0.15, and 0.34 $cm^2 V^{-1} s^{-1}$ to 0.18, 0.58, 0.87, 0.011, and 0.022 $cm^2 V^{-1} s^{-1}$, respectively. Accordingly, the air-stability of tetrachlorinated NDIs was worse than that for NDIs with two Cl substituents, regardless of their lower LUMO levels. As shown by single-crystal analysis (see further), this is closely related to the fact that NDIs with two Cl substituents have an undistorted π-conjugated core and show more densely packed fluorocarbon chains compared to those with four Cl substituents. NDIs with two Cl substituents benefit from the viewpoint of kinetic barrier mechanisms.

The hysteresis of **3b** TFTs was examined both in N_2 and in air. Figure 3 shows the bidirectional transfer and output plots. In N_2 atmosphere, TFTs of **3b** exhibited a minimal hysteresis for transfer and output characteristics. On the other hand, in ambient air, the hysteresis increased to some degree because of trapping of the charge carriers by ambient oxidants, with a V_T shift of less than +10 V. The relatively high V_T may be decreased by optimizing the contact behavior or tuning the capacitance of the dielectric layer. Compound **4b**, containing four Cl substituents at the core and a $-CH_2C_4F_9$ group at the imide nitrogen, showed higher mobilities compared to **4a** with four Cl substituents and a $-CH_2C_3F_7$ group at the imide nitrogen. The best performance for TFTs of **4b** was obtained (0.44 $cm^2 V^{-1} s^{-1}$) on OTS-treated SiO_2/Si substrates at $T_D = 70$ °C.

It is noteworthy that the best performance for **3b** and **4b** thin films, which have five carbons in the fluoroalkyl chains, was obtained at the higher T_D (70 °C) and on OTS-treated SiO_2/Si substrates, whereas for **3a** and **4a** films, with four carbons in the

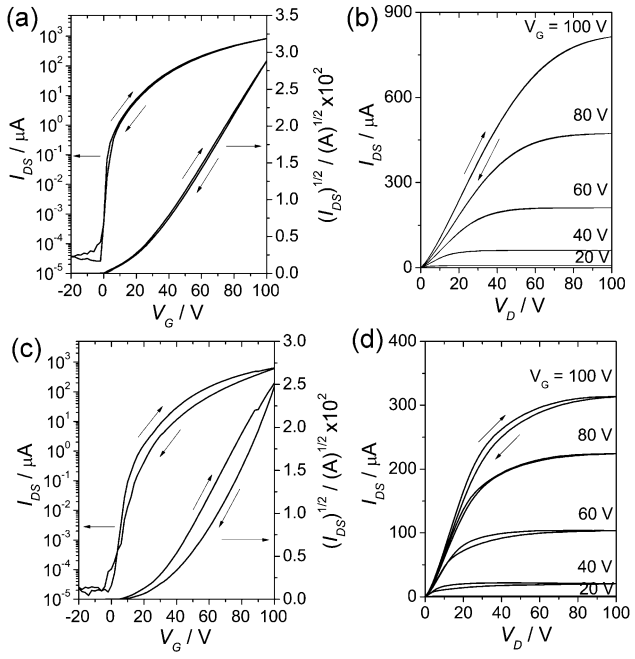

Figure 3. Bidirectional transfer and output plots for a TFT prepared from compound **3b** on OTS-treated SiO_2/Si substrate at $T_D = 70$ °C in N_2 and air: a) transfer plot in N_2, b) output plot in N_2, c) transfer plot in air, and d) output plot in air. The forward and reverse sweeps are indicated by respective arrows.

fluoroalkyl chains, the best performance was obtained at the lower T_D (50 °C) and on the bare SiO_2/Si substrate. In addition, TFTs made from NDIs **3b** and **4b** (with longer side chains) showed slightly higher mobilities. This is opposite to the results reported for PDI semiconductors with the same fluoroalkyl side chains.[17,18] A PDI derivative with $CH_2C_3F_7$ imide chains yielded an order of magnitude higher mobility compared to that with $CH_2C_4F_9$ imide substituents. Locklin et al. found that the relative ratio of the size of the end group with regard to the size of the inner semiconducting core of the molecule is an important factor in orienting the molecule in the thin-film phase.[35] The different TFT characteristics observed for NDIs **3a** and **3b** clearly reveal a subtle influence of the substrate and the deposition temperature on the molecular organization in the NDI thin films despite of the rather similar packing of the NDI cores in the single crystals.

The chlorinated NDIs are highly soluble in chlorinated solvents such as chloroform and *o*-dichlorobenzene, indicating that these NDI semiconductors hold benefits in terms of their processing versatility. To investigate the processing versatility of these NDI semiconductors, preliminary studies were performed using spin-coating and shearing[36] methods. Typically, spin-coated devices displayed mobilities of 10^{-3}–10^{-5} $cm^2 V^{-1} s^{-1}$, whereas shearing devices yielded mobilities of 10^{-2}–10^{-3} $cm^2 V^{-1} s^{-1}$. Further optimization of the device structure and performance for solution-processed TFTs is required and will be reported in due course.

2.4. Thin Film X-Ray Diffraction (XRD)

To obtain information on the molecular order and orientations relative to the substrate surfaces, XRD experiments were carried out on 45-nm-thick NDI thin films prepared under the same evaporation condition as the TFT devices. The XRD patterns and the peak assignments are available in the Supporting Information (Fig. S2 and Table S2). The out-of-plane *d*(001)-spacing data are listed in Table 3. The well-defined XRD peaks for the NDI derivatives indicate highly ordered/layered microstructures in all films. The out-of-plane *d*(001)-spacing (16.7 Å) of compound **2a** was very close to that (17 Å) previously reported.[9] In addition, for all NDI thin films, the *d*(001)-spacing values were similar to the geometry-optimized, calculated molecular lengths obtained from MM2 energy-minimization and PM3 geometry-optimization calculations. This indicates that the NDI molecules adopt an edge-on conformation in the thin films. In general, PDI thin films deposited on OTS-treated SiO_2 substrates exhibit higher intensities of the XRD peaks compared to those on bare SiO_2 substrates, which is consistent with the observation of larger grain sizes and, as a result, higher charge-carrier mobilities.[13,18,32] In addition, thin-film deposition at higher substrate temperature (T_D) (however, not surpassing the desorption temperature) yields a higher degree of crystallinity in the films.[10,17] Interestingly, unlike the results for PDI thin films, we observed high-intensity diffraction peaks with narrow full width at half-maximum (FWHM) values for the NDI thin films prepared on bare SiO_2 substrates as well as for those prepared at low substrate temperatures (25 °C). This agrees well with the high mobilities found for these NDI compounds on bare SiO_2/Si substrates. As the NDI molecules have a relatively smaller core size, they were less sensitive to the surface treatment, which means that they are simpler to process compared to their PDI counterparts.

Table 3. Thin-film X-ray diffraction (XRD) and molecular length data for NDI semiconductors.

Semiconductor	T_D [°C]	*d*(001)-spacing [Å] [a]	Calculated molecular length [Å] [b]	Single crystal molecular length [Å] [c]
2a	25	16.72	18.43	–
3a	50	19.28	18.44	18.75
3b	25	21.48	20.49	21.31
4a	70	18.39	18.31	19.02
4b	50	20.25	20.44	21.68

[a] 45-nm thin films were analyzed with Cu Kα radiation at a power of 45 mV and 40 mA, with a step size of 0.02° and a step time of 1.0 s. [b] Geometry-optimized, molecular lengths obtained from MM2 energy minimization and PM3 geometry optimization calculations. [c] Molecular lengths obtained from single-crystal X-ray diffraction analysis.

2.5. Molecular Packing in the Solid State

To achieve a better understanding of the molecular arrangement in the solid state and its consequences for charge transport, solvent-free single crystals of the chlorinated NDIs were obtained by recrystallization, and their structures were investigated using single-crystal X-ray diffraction. The dichlorinated NDI derivative **3a** crystallizes in the monoclinic space group $P2_1/c$. The unit cell packing viewed along the *a*-axis is illustrated in Figure 4a. The crystal structure of **3a** shows a slip-stacked edge-to-face herringbone arrangement with cell parameters $a = 11.870$ Å, $b = 16.633$ Å, $c = 5.935$ Å, $\alpha = \gamma = 90°$, $\beta = 104.42°$, and $Z = 2$. It is well known that a herringbone structure can be observed when two adjacent molecular stacks have a roll angle in the opposite direction.[37] A herringbone motif with the same space group has also been observed for a difluorinated PDI derivative with the same fluoroalkyl chain.[18] Figure 4b, viewed along the *b*-axis, depicts the segregation of the arene and fluoroalkyl groups. The self-segregation of densely packed fluorocarbon chains is generally known to improve the air-stability of n-channel OTFT devices by providing a kinetic barrier to the diffusion of ambient oxidants into the active channel area.[1,12,17–19] The distortion of the NDI core is marginal (Fig. 4c), indicating a high degree of planarity of the π-conjugated backbone in the solid state in contrast to previously reported core-halogenated PDIs.[16,18] The single crystal of **3a** exhibits a close interplanar spacing of 3.338 Å between the stacks (Fig. 4d). The slipping angle of the stack is 62°. This is larger than that (39°) of the corresponding PDI with two F substituents at the core, meaning that the overlap of the π-conjugated core is substantially increased along the stacking direction. The closest distance between neighboring molecules is 2.357 Å (O-H contacts between imide oxygens and hydrogens of the fluoroalkyl group). Detailed crystallographic data is given in the Supporting Information (see Table S3).

Compound **3b**, having one additional difluoromethylene unit at the imide substituent compared to **3a**, crystallizes in the same space group $P2_1/c$ with unit cell parameters $a = 11.703$ Å, $b = 16.842$ Å, $c = 6.531$ Å, $\alpha = \gamma = 90°$, $\beta = 99.518°$, and $Z = 2$ (Fig. S3a). Notably, an almost identical packing of the NDI cores is observed with well-defined segregation of the arene and fluoroalkyl groups (Fig. S3b) revealing a nearly negligible influence of the additional CF_2 group on the single crystal packing. Thus, the *a*- and *b*-parameters of the unit cells of **3a** and **3b** are virtually identical and only the *c*-parameters are different because this is the direction in which the additional CF_2 group is embedded. The NDI core in **3b** is nearly planar with a torsion angle of only about 0.5–1° with a close interplanar spacing of 3.423 Å and the same slipping angle (62°) of the stacks as that for **3a** (Fig. S3c and d). The single-crystal features of **3a** and **3b**, namely, their high planarity, very close distance of the π-conjugated NDI cores, and their high calculated density of the crystal structures (2.046–2.091 g cm^{-3}) account for their high charge-carrier mobilities.

The crystal structure of **4a** with four Cl substituents at the NDI core exhibits a triclinic space group *P*-1 with unit cell parameters of $a = 5.104$ Å, $b = 10.358$ Å, $c = 12.395$ Å, $\alpha = 111.08°$, $\beta = 90.07°$, $\gamma = 96.67°$, and $Z = 1$ (Fig. 5). The distortion of the naphthalene π-conjugated core is more pronounced (dihedral angles up to 7.2°, see Fig. 5c) than that of the dichlorinated derivatives but it is still much smaller than the distortion of tetrafluorinated PDIs (ca. 25°) or tetrachlorinated PDIs (ca. 35°).[16,18] Thus, in contrast to the presence of complex packing patterns for tetrahalogenated PDIs because of *M*/*P*-atropisomerism, simple slip-stacked face-to-face molecular packing is still possible for tetrachlorinated NDIs (Fig. 5d) despite the larger distance (3.463 Å) between the π-planes

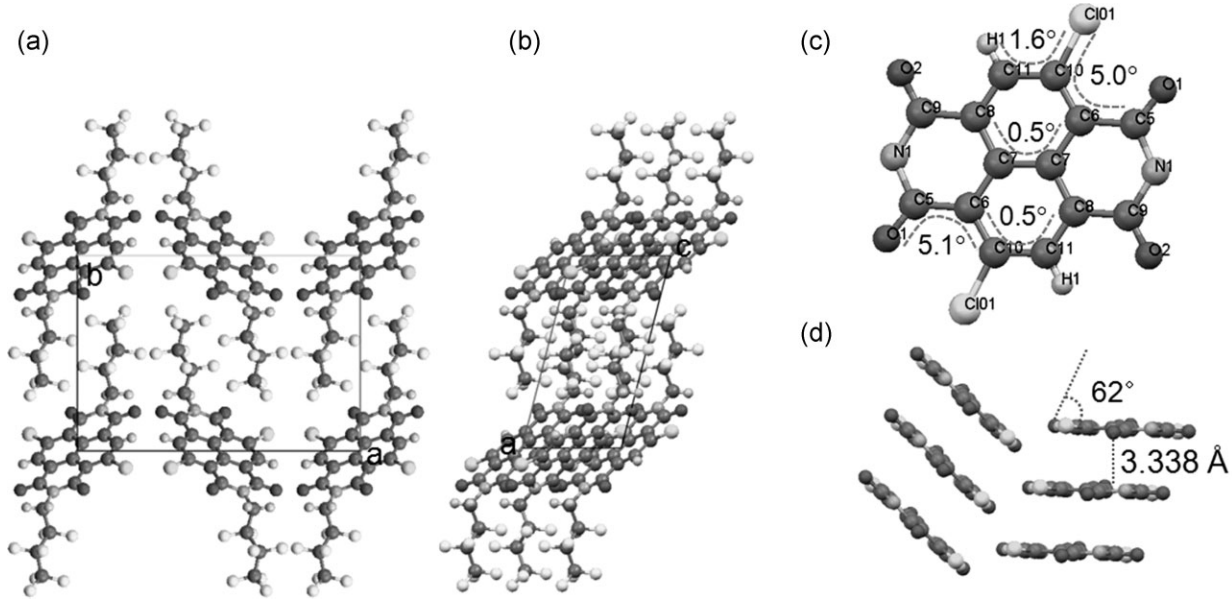

Figure 4. Single-crystal structure of **3a**. Unit-cell packing ($a = 11.870$ Å, $b = 16.633$ Å, $c = 5.935$ Å, $\alpha = \gamma = 90°$, $\beta = 104.42°$, and $Z = 2$) viewed along different directions: a) a-axis and b) b-axis. The latter shows the segregation of the arene and fluoroalkyl groups. c) NDI core with labeled atoms and dihedral angles. d) Side view on the stacks with π-plane distance and angle (for clarity, only the naphthalene part is shown in (c) and (d)).

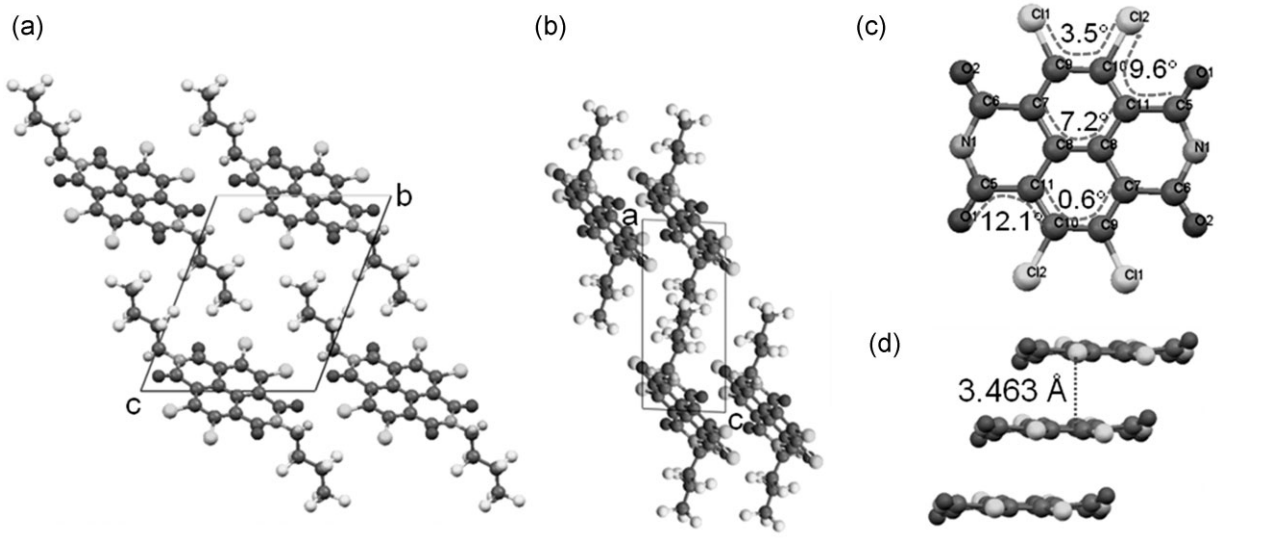

Figure 5. Single-crystal structure of **4a**. Unit cell packing ($a = 5.104$ Å, $b = 10.358$ Å, $c = 12.395$ Å, $\alpha = 111.08°$, $\beta = 90.07°$, $\gamma = 96.67°$, and $Z = 1$) viewed along different directions: a) a-axis and b) b-axis. c) NDI core with labeled atoms and dihedral angles. d) Side view on the stacks with π-plane distance and angle (for clarity, only the naphthalene part is shown in (c) and (d)).

as compared to the dichlorinated derivatives. Therefore, **4a** should also show high charge-carrier mobilities in the well-ordered solid state. The LUMO level of **4a** with four Cl substituents was lower by 0.12 eV compared to that of **3a** with two Cl substituents. However, as can be seen from Figure 5b, the packing density of the fluorinated side chains in the **4a** crystal was lower than that in the **3a** crystal. The lower air-stability of **4a** can thus be attributed to unfavorable kinetic factors.

The crystal of **4b** with four Cl substituents shows a triclinic space group *P*-1 (Fig. S4), similar to that of **4a**. The unit cell parameters are $a = 5.506$ Å, $b = 9.810$ Å, $c = 12.707$ Å, $\alpha = 87.79°$, $\beta = 81.09°$, $\gamma = 87.29°$, and $Z = 1$. The π-conjugated core is fairly planar (torsion angle $< 5°$) and the π-plane distance is 3.438 Å, indicating that **4b** should give high mobilities in the solid state. Similar to the case of **3a** and **4a**, the packing density of the fluorinated side chains in the crystal of **4b** became less than that in crystals of **3b**, resulting in a reduced air-stability of **4b**.

2.6. AFM Analysis

To elucidate the unusual higher mobilities of **3a** and **4a** on bare SiO_2/Si substrates at an elevated T_D as well as the superior performance of **3b**, the thin-film growth and morphologies were studied using atomic force microscopy (AFM) analysis. Figure 6a and b exhibit the AFM topography images of thin films of compound **3a** prepared at 25 °C on OTS-treated SiO_2/Si and bare SiO_2/Si substrates, respectively. The average length of the long axis of the grains of compound **3a** was around 140 nm for the film on the bare SiO_2/Si substrate compared to around 620 nm for the film on the OTS-treated SiO_2/Si substrate. However, at an elevated T_D of 50 °C, the grains in the thin films of compound **3a** on bare SiO_2/Si substrates became larger (ca. 1.3 μm in the long axis of the grain) than those (ca. 0.8 μm) on OTS-treated SiO_2/Si substrates, as can be seen from Figure 6c and d. This corresponds well to the results of the OTFT performance and the XRD analysis. It is well known that charge transport in an OTFT device takes place predominantly in the first few monolayers (MLs) of the organic semiconductor near the semiconductor/dielectric interface.[5,38,39] To investigate the influence of the substrate on the film growth of charge

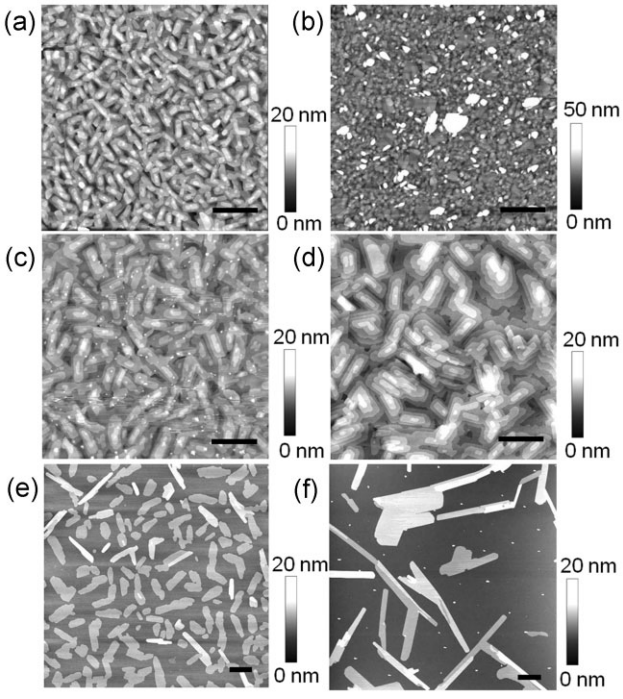

Figure 6. AFM topography images of compound **3a** thin films prepared under different conditions: a) OTS-treated SiO_2/Si substrate at 25 °C, b) bare SiO_2/Si substrate at 25 °C, c) OTS-treated SiO_2/Si substrate at 50 °C, d) bare SiO_2/Si substrate at 50 °C (films (a–d) had a nominal thickness of 45 nm), e) 3 nm nominal thickness on OTS-treated SiO_2/Si substrate at 50 °C, and f) 3 nm nominal thickness on bare SiO_2/Si substrate at 50 °C. The scale bar is 1 μm.

accumulation layers, we prepared **3a** thin films with a nominal thickness of 3 nm on OTS-treated SiO_2/Si and on bare SiO_2/Si substrates at 50 °C (Fig. 6e and f). On the bare SiO_2/Si substrate, compound **3a** formed larger grains but with similar height compared to the grains on the OTS-treated SiO_2/Si substrate. The formation of less grain boundaries may also explain the higher charge-carrier mobility for the films deposited on bare SiO_2/Si under these conditions.

Thin films of **4a** formed microfibrillar grains that were slightly longer (ca. 1.1 μm) on the OTS-treated SiO_2/Si substrate than those (ca. 0.8 μm) on the bare SiO_2/Si substrate at a T_D of 25 °C (Fig. S5). However, at an elevated T_D of 70 °C, the grain sizes on the bare SiO_2/Si became larger (ca. 3.5 μm) than those (ca. 2.7 μm) on the OTS-treated SiO_2/Si, leading to a higher mobility on the bare SiO_2/Si. On the other hand, **3b** thin films prepared under optimized deposition conditions showed grains with a significantly larger area (up to one and a half times) compared to those in optimized **3a** and **4a** thin films, which is consistent with the superior performance of **3b** (Fig. S6).

In general, however, the thin-film growth of core-chlorinated NDI compounds was less sensitive to surface modification of the dielectric and to the substrate temperature, compared to PDI molecules[16–18] as their thin films already contain large grains even on bare SiO_2/Si substrates and at relatively low substrate temperatures. In addition, they are highly soluble in common organic solvents, indicating a better processing versatility compared to their PDI counterparts. These factors make core-chlorinated NDIs highly promising candidates for high-performance n-channel OTFTs.

3. Conclusions

We described the synthesis and structural analyses of core-chlorinated NDIs with two different fluorinated side chains at the imide nitrogen, and characterized their electrical properties as n-channel semiconductors. The LUMO level and bandgap of the NDI molecules gradually decreased as the degree of chlorination increased. Unlike the severe core-twisting of core-halogenated PDI molecules, however, our core-functionalized NDIs showed an excellent planarity of the π-conjugated core, which is beneficial to charge transport. The dichlorinated NDIs adopted a slip-stacked edge-to-face herringbone arrangement with well-defined segregation of the arene and fluoroalkyl groups. The distance between the π-planes was very small (3.3–3.4 Å) and a large overlap between the π-stacks was observed with a slipping angle of around 62°. Dichlorinated NDI **3b** exhibited the best field-effect mobility (up to 1.43 $cm^2 V^{-1} s^{-1}$) together with minimal hysteresis and high on–off ratios (ca. 10^7) in air. High field-effect mobilities (up to 0.44 $cm^2 V^{-1} s^{-1}$) were also obtained from tetrachlorinated NDI **4b**. Interestingly, **3b** and **4b** with five (odd number) carbons in the fluoroalkyl chains gave the best performance at higher T_D (70 °C) and on an OTS-treated SiO_2 dielectric, whereas **3a** and **4a** with four (even number) carbons in the fluoroalkyl chains showed their optimal performance at lower T_D (50 °C) and on a bare SiO_2 dielectric surface. In contrast to their PDI analogues, **3b** and **4b** (with longer side chains) yielded higher mobilities. This may be related to the fact that the molecular packing and concomitant charge-transport behavior is highly sensitive to the relative ratio of the size of the end group with regard to that of the π-conjugated core. The air-stability of NDIs with two Cl substituents was better than of those with four Cl substituents, despite their higher LUMO. This can be explained by the denser packing of the fluorocarbon chains in NDIs with two Cl substituents, which serves as a kinetic barrier to the diffusion of ambient oxidants. Core-chlorinated NDIs are found to be highly promising n-channel candidates for practical applications in low-cost, large-area, flexible electronics, because of their straightforward synthesis, processing versatility, high-performance, and good air-stability.

4. Experimental

Instrumentation: Cyclic-voltammetry experiments were performed using a standard commercial electrochemical analyzer (EC epsilon; BAS Instruments, UK) with a three-electrode single-compartment cell under argon. Dichloromethane (HPLC grade) was dried over calcium hydride under argon and degassed before use. The supporting electrolyte, tetrabutylammonium hexafluorophosphate (TBAHFP), was prepared according to the literature [40], recrystallized from an ethanol/water mixture, and dried under vacuum. The measurements were carried out in dichloromethane at a concentration of about 10^{-4} M with ferrocene (Fc) as the internal standard for the calibration of the potential. Ag/AgCl was used as the reference electrode and a Pt disc and a Pt wire were used as the working and auxiliary electrodes, respectively. UV-vis spectra were recorded with a Varian Cary 6000i UV-vis spectrophotometer. All solutions were prepared using *o*-dichlorobenzene under ambient conditions, whereas thin films were vacuum-deposited on a quartz plate. A Philips PANalytical X'Pert diffractometer with a PreFIX X-ray mirror at the incident-beam side and a parallel-plate collimator at the diffracted-beam side was used to obtain diffraction patterns from thin films of the evaporated molecules. $2\theta/\omega$ scans were carried out using Cu Kα radiation at a power of 45 mV and 40 mA, with a step size of 0.02°, and a step time of 1.0 s. Single-crystal X-ray diffraction (XRD) data were collected using a Bruker D8/Apex diffractometer with a CCD area detector and graphite monochromated or multilayer mirror monochromated Mo Kα radiation. A Digital Instruments (DI) MMAFM-2 scanning probe microscope was used to perform tapping-mode atomic force microscopy (AFM) on the samples with a silicon tip frequency of 300 kHz. DI Nanoscope software was used to process the raw AFM images.

Device Fabrication and Characterization: Transistor devices with bottom-gate top-contact configuration were prepared to characterize the performance of NDI-based TFTs. Highly doped n-type (100) silicon wafers with thermally grown SiO_2 (300 nm thickness, capacitance per unit area (C_i): 1.0×10^{-8} F cm^{-2}) were used as the substrates. The SiO_2/Si wafers were cleaned with a piranha solution (H_2SO_4/H_2O_2, 70:30, v/v) for 30 min, then rinsed thoroughly with deionized water, and dried using a nitrogen gun (99.9% pure N_2). The SiO_2/Si substrates were subsequently treated with UV-ozone plasma (Jetlight UVO-cleaner Model 42–100V) for 20 min. Octadecyltrimethoxysilane (OTS) treatment was carried out according to a previously published procedure, which forms crystalline OTS by spin-coating [34]. The SiO_2/Si substrates were spin-coated from a 3 mM solution of OTS in trichloroethylene, and placed in an environment saturated with ammonia vapor for 12 h, followed by sonication cleaning, sequential washing, and drying. The organic semiconductors were vacuum-deposited at a rate of 0.2–0.3 Å s^{-1} under a pressure of around 1×10^{-6} Torr to their target thickness (45 nm) as determined in-situ by a calibrated quartz crystal microbalance (QCM). Gold was thermally evaporated onto the semiconductor layer to form source and drain electrodes using shadow masks with a channel width (W) to length (L) ratio (W/L) of 20 ($W = 1000$ μm, $L = 50$ μm or $W = 2000$ μm, $L = 100$ μm). The current–voltage (I–V) characteristics of the devices were measured either in air (ambient lab environment) or in a nitrogen glovebox (oxygen level < 1 ppm) using a Keithley 4200-SCS semiconductor parameter analyzer. Key device parameters, such as the field-effect mobility (μ), on–off current ratio (I_{on}/I_{off}),

and the threshold voltage (V_T) were extracted from the drain–source current (I_{DS}) versus gate voltage (V_G) characteristics using conventional transistor equations [38]:

$$I_{DS} = \frac{W}{2L}\mu C_i(V_G - V_T)^2 \quad (1)$$

The mobility was determined in the saturation regime from the slope of plots of $(I_{DS})^{1/2}$ versus V_G.

Crystallographic data for the structures reported in this paper have been deposited with the Cambridge Crystallographic Data Centre as supplementary publication no. CCDC-761579 to CCDC-761582 (see Table S3 in the Supporting Information).

Acknowledgements

Z.B. and F.W. acknowledge the financial support from BASF SE. Z.B. acknowledges the NSF-DMR for solid-state chemistry, the Sloan Research Fellowship, and the Center for Polymeric Interfaces and Macromolecular Assemblies (NSF-Center MRSEC under Award Number DMR-0213618). Supporting information is available online from Wiley InterScience or from the author.

Received: March 6, 2010
Published online: June 14, 2010

[1] H. E. Katz, Z. N. Bao, S. L. Gilat, *Acc. Chem. Res.* **2001**, *34*, 359.
[2] C. R. Newman, C. D. Frisbie, D. A. da Silva, J.-L. Brédas, P. C. Ewbank, K. R. Mann, *Chem. Mater.* **2004**, *16*, 4436.
[3] J.-L. Brédas, D. Beljonne, V. Coropceanu, J. Cornil, *Chem. Rev.* **2004**, *104*, 4971.
[4] J. E. Anthony, *Chem. Rev.* **2006**, *106*, 5028.
[5] Z. Bao, J. Locklin, *Organic Field-Effect Transistors*, Vol. *1*, Taylor, Boca Raton, FL **2007**.
[6] D. Braga, G. Horowitz, *Adv. Mater.* **2009**, *21*, 1473.
[7] H. Yan, Z. Chen, Y. Zheng, C. Newman, J. R. Quinn, F. Dotz, M. Kastler, A. Facchetti, *Nature* **2009**, *457*, 679.
[8] L. L. Chua, J. Zaumseil, J. F. Chang, E. C. W. Ou, P. K. H. Ho, H. Sirringhaus, R. H. Friend, *Nature* **2005**, *434*, 194.
[9] H. E. Katz, A. J. Lovinger, J. Johnson, C. Kloc, T. Siegrist, W. Li, Y. Y. Lin, A. Dodabalapur, *Nature* **2000**, *404*, 478.
[10] R. J. Chesterfield, J. C. McKeen, C. R. Newman, P. C. Ewbank, D. A. da Silva, J.-L. Brédas, L. L. Miller, K. R. Mann, C. D. Frisbie, *J. Phys. Chem. B* **2004**, *108*, 19281.
[11] A. Facchetti, M. H. Yoon, C. L. Stern, G. R. Hutchison, M. A. Ratner, T. J. Marks, *J. Am. Chem. Soc.* **2004**, *126*, 13480.
[12] B. A. Jones, M. J. Ahrens, M. H. Yoon, A. Facchetti, T. J. Marks, M. R. Wasielewski, *Angew. Chem. Int. Ed.* **2004**, *43*, 6363.
[13] B. A. Jones, A. Facchetti, M. R. Wasielewski, T. J. Marks, *J. Am. Chem. Soc.* **2007**, *129*, 15259.
[14] A. F. Brooks, A. Jones, M. R. Wasielewski, T. J. Marks, *Adv. Funct. Mater.* **2008**, *18*, 1329.
[15] R. T. Weitz, K. Amsharov, U. Zschieschang, E. B. Villas, D. K. Goswami, M. Burghard, H. Dosch, M. Jansen, K. Kern, H. Klauk, *J. Am. Chem. Soc.* **2008**, *130*, 4637.
[16] R. Schmidt, M. M. Ling, J. H. Oh, M. Winkler, M. Könemann, Z. N. Bao, F. Würthner, *Adv. Mater.* **2007**, *19*, 3692.
[17] J. H. Oh, S. Liu, Z. Bao, R. Schmidt, F. Würthner, *Appl. Phys. Lett.* **2007**, *91*, 212107.
[18] R. Schmidt, J. H. Oh, Y.-S. Sun, M. Deppisch, A.-M. Krause, K. Radacki, H. Braunschweig, M. Könemann, P. Erk, Z. Bao, F. Würthner, *J. Am. Chem. Soc.* **2009**, *131*, 6215.
[19] H. E. Katz, J. Johnson, A. J. Lovinger, W. Li, *J. Am. Chem. Soc.* **2000**, *122*, 7787.
[20] X. Gao, C-a. Di, Y. Hu, X. Yang, H. Fan, F. Zhang, Y. Liu, H. Li, D. Zhu, *J. Am. Chem. Soc.* **2010**, *132*, 3697.
[21] B. J. Jung, J. Sun, T. Lee, A. Sarjeant, H. E. Katz, *Chem. Mater.* **2009**, *21*, 94.
[22] Y.-L. Lee, H.-L. Hsu, S.-Y. Chen, T.-R. Yew, *J. Phys. Chem. C* **2008**, *112*, 1694.
[23] D. Shukla, S. F. Nelson, D. C. Freeman, M. Rajeswaran, W. G. Ahearn, D. M. Meyer, J. T. Carey, *Chem. Mater.* **2008**, *20*, 7486.
[24] Z. Bao, A. J. Lovinger, J. Brown, *J. Am. Chem. Soc.* **1998**, *120*, 207.
[25] M. H. Yoon, S. A. DiBenedetto, A. Facchetti, T. J. Marks, *J. Am. Chem. Soc.* **2005**, *127*, 1348.
[26] M. H. Yoon, A. Facchetti, C. E. Stern, T. J. Marks, *J. Am. Chem. Soc.* **2006**, *128*, 5792.
[27] A. Facchetti, M. Mushrush, H. E. Katz, T. J. Marks, *Adv. Mater.* **2003**, *15*, 33.
[28] J. H. Oh, Y.-S. Sun, R. Schmidt, M. F. Toney, D. Nordlund, M. Könemann, F. Würthner, Z. Bao, *Chem. Mater.* **2009**, *21*, 5508.
[29] M. L. Tang, J. H. Oh, A. D. Reichardt, Z. Bao, *J. Am. Chem. Soc.* **2009**, *131*, 3733.
[30] M. Gsänger, J. H. Oh, M. Könemann, H. W. Höffken, A.-M. Krause, Z. Bao, F. Würthner, *Angew. Chem. Int. Ed.* **2010**, *49*, 740.
[31] C. Thalacker, C. Röger, F. Würthner, *J. Org. Chem.* **2006**, *71*, 8098.
[32] M. M. Ling, P. Erk, M. Gomez, M. Koenemann, J. Locklin, Z. N. Bao, *Adv. Mater.* **2007**, *19*, 1123.
[33] M. J. Frisch, G. W. Trucks, H. B. Schlegel, G. E. Scuseria, M. A. Robb, J. R. Cheeseman, J. A. Montgomery, Jr, T. Vreven, K. N. Kudin, J. C. Burant, J. M. Millam, S. S. Iyengar, J. Tomasi, V. Barone, B. Mennucci, M. Cossi, G. Scalmani, N. Rega, G. A. Petersson, H. Nakatsuji, M. Hada, M. Ehara, K. Toyota, R. Fukuda, J. Hasegawa, M. Ishida, T. Nakajima, Y. Honda, O. Kitao, H. Nakai, M. Klene, X. Li, J. E. Knox, H. P. Hratchian, J. B. Cross, V. Bakken, C. Adamo, J. Jaramillo, R. Gomperts, R. E. Stratmann, O. Yazyev, A. J. Austin, R. Cammi, C. Pomelli, J. W. Ochterski, P. Y. Ayala, K. Morokuma, G. A. Voth, P. Salvador, J. J. Dannenberg, V. G. Zakrzewski, S. Dapprich, A. D. Daniels, M. C. Strain, O. Farkas, D. K. Malick, A. D. Rabuck, K. Raghavachari, J. B. Foresman, J. V. Ortiz, Q. Cui, A. G. Baboul, S. Clifford, J. Cioslowski, B. B. Stefanov, G. Liu, A. Liashenko, P. Piskorz, I. Komaromi, R. L. Martin, D. J. Fox, T. Keith, M. A. Al-Laham, C. Y. Peng, A. Nanayakkara, M. Challacombe, P. M. W. Gill, B. Johnson, W. Chen, M. W. Wong, C. Gonzalez, J. A. Pople, Gaussian 03, Revision C.01, Gaussian Inc, Wallingford, CT **2004**.
[34] Y. Ito, A. A. Virkar, S. Mannsfeld, J. H. Oh, M. Toney, J. Locklin, Z. Bao, *J. Am. Chem. Soc.* **2009**, *131*, 9396.
[35] J. Locklin, D. Li, S. C. B. Mannsfeld, E.-J. Borkent, H. Meng, R. Advincula, Z. Bao, *Chem. Mater.* **2005**, *17*, 3366.
[36] H. A. Becerril, M. E. Roberts, Z. Liu, J. Locklin, Z. Bao, *Adv. Mater.* **2008**, *20*, 2588.
[37] M. D. Curtis, J. Cao, J. W. Kampf, *J. Am. Chem. Soc.* **2004**, *126*, 4318.
[38] V. Coropceanu, J. Cornil, D. A. da Silva Filho, Y. Olivier, R. Silbey, J.-L. Brédas, *Chem. Rev.* **2007**, *107*, 926.
[39] A. Dodabalapur, L. Torsi, H. E. Katz, *Science* **1995**, *268*, 270.
[40] A. J. Fry, *Laboratory Techniques in Electroanalytical Chemistry*, Marcel Dekker Ltd., New York, NJ **1996**.